Causal Epigenetic Age Uncouples Damage and Adaptation

Kejun Ying[1,2], Hanna Liu[1,3], Andrei E. Tarkhov[1], Ake T. Lu[4,5], Steve Horvath[4,5], Zoltán Kutalik[6], Xia Shen[7], Vadim N. Gladyshev[1,✉]

[1] Division of Genetics, Department of Medicine, Brigham and Women's Hospital and Harvard Medical School, Boston, MA, USA

[2] T. H. Chan School of Public Health, Harvard University, Boston, MA, USA

[3] Massachusetts College of Pharmacy and Health Sciences, Boston, MA, USA

[4] Altos Labs, San Diego, CA, USA

[5] Departments of Human Genetics and Biostatistics, University of California, Los Angeles, CA, USA

[6] University Center for Primary Care and Public Health, University of Lausanne, Lausanne, Switzerland

[7] Greater Bay Area Institute of Precision Medicine (Guangzhou), Fudan University, Guangzhou, China

✉ email: vgladyshev@rics.bwh.harvard.edu

Abstract

Machine learning models based on DNA methylation can be used to predict the age of biological samples, but their interpretability is limited due to the lack of causal inferences. Here, we leveraged large-scale genetic data and performed epigenome-wide Mendelian Randomization to identify CpG sites causal to aging-related traits. We show that neither the existing epigenetic clocks nor DNA methylation changes are enriched in causal CpG sites. Causal CpGs include similar numbers of sites that contribute to aging and protect against it, yet their combined contribution negatively affects age-related traits. We developed a framework for integrating causal knowledge into epigenetic clock models and constructed *DamAge* and *AdaptAge* that measure age-related damaging and adaptive changes, respectively. *DamAge* acceleration is associated with various adverse conditions (e.g., mortality risk), whereas *AdaptAge* acceleration is related to beneficial adaptations. Only *DamAge* is reversed upon cell reprogramming. Our results offer a comprehensive map of CpG sites causal to lifespan and healthspan, allowing to build causal biomarkers of aging and rejuvenation and assess longevity interventions, age reversal, and aging-accelerating events.

Introduction

Aging is a complex biological process characterized by a buildup of deleterious molecular changes that result in a gradual decline of function of various organs and systems and ultimately lead to death [1]. Although the underlying mechanisms of aging are not well understood, various studies indicate that aging is strongly associated with changes in the epigenome, quantified as a set of chemical modifications to DNA and histones that affect gene expression and chromatin structure [2]. DNA methylation is one of the best studied epigenetic modifications. In mammals, 5-methylcytosine (5mC) is the most common form of DNA methylation, which is achieved by the action of DNA methyltransferases (DNMTs) [3,4]. Studies have shown that DNA methylation patterns change with age, wherein the global level of DNA methylation decreases slightly during adulthood, while some local areas may be hypomethylated or hypermethylated [2,5–8]. Furthermore, the level of methylation of some specific CpG sites shows a strong correlation with age, which can be used to build machine learning-based models that can accurately predict the age of biological samples [7,9]. As models can quantify age with very high accuracy, researchers termed these models epigenetic aging clocks (e.g., Horvath pan tissue epigenetic clock and Hannum blood based epigenetic clock) [10,11]. The predicted age based on various epigenetic aging clocks appears to have a higher association with health-related measurements than chronological age. Therefore, it is believed that they could be used to better represent the biological age of samples than chronological age [12].

Although epigenetic aging clocks provide a useful tool for profiling biological aging, they should be used with caution, as they are built based on pure correlations [13]. It is unclear whether the DNA methylation changes that are used to predict age are causal to aging-related phenotypes or are simply byproducts of the aging process that does not influence aging themselves. To establish a causal relationship, the gold standard approach is the application of randomized controlled trials (RCT), where participants are randomly assigned to the intervention arm that receives the treatment or the control arm. As the randomization step balances all confounding factors between two arms, the differences observed in the outcome between two groups are purely driven by the intervention; thus, the causal effect can be estimated [14]. However, given the large number of CpG sites across the genome, it is inefficient and infeasible to perform the perturbation on each of them and assess the aging-related outcomes.

Mendelian randomization (MR) is a genetic approach to causal inference that recapitulates the principle of RCT. Instead of perturbing an exposure through treatment, the MR uses the genetic variants that are robustly associated with the exposure as instrumental variables [15,16]. As genetic variants of parental DNA are naturally randomly passed on to the offspring, the effect estimated by MR is not affected by environmental confounders and thus can be considered as an estimation of a causal effect, similar to the RCTs. In recent years, several studies have shown that MR can be applied to molecular traits by using the genetic variants associated with molecular levels as instruments (also known as molecular quantitative trait loci, molQTL) [17]. These molecular QTLs include gene expression (eQTL) [18], RNA splicing (sQTL) [19], plasma protein (pQTL) [20], metabolites (mQTL) [21], as well as DNA methylation (meQTL) [22]. A previous study showed that it is feasible to use meQTLs as instruments to identify causal CpG sites for diseases [23]. By integrating molQTLs with genome-wide association studies for traits such as lifespan, healthspan, extreme longevity, and other measurements related to aging, it is biologically plausible to perform two-sample MR to estimate the causal effects of molecular changes on the aging process.

Here, we leveraged large-scale genetic data and performed epigenome-wide Mendelian Randomization (EWMR) on 420,509 CpG sites to identify CpG sites that are causal to twelve aging-related traits. We found that none of the existing clocks are enriched for causal CpG sites. We further constructed a causality-informed clock based on this inferred causal knowledge, as well as clocks that separately measure damaging and protective changes. Their applications provide direct insights into the aging process. Thus, our results offer a comprehensive map of human CpG sites causal to aging traits, which can be used to build causal biomarkers of aging and assess novel anti-aging interventions and aging-accelerating events.

Results

Epigenome-wide Mendelian Randomization on aging-related phenotypes

MR is an established genetic approach for causal inference that utilizes natural genetic variants as instrument variables. Since the allocation of genetic variants is a random process and is determined during conception, the causal effects estimated using MR are not biased by environmental confounders. Therefore, it could be used as a tool for investigating causal relationships between the DNA methylation and aging-related phenotypes (Fig. 1a). To identify CpG sites causal to

aging, we used 420,509 CpG sites with meQTLs available (GoDMC, whole blood samples from 36 cohorts, 27,750 European subjects) as exposures and selected twelve aging-related phenotypes as outcomes (Fig. 1a, Methods), including two lifespan-related traits (lifespan and extreme longevity) [24], three health-related traits (healthspan, frailty index, and self-rated health) [25,26], four epigenetic age measurements (Horvath age, Hannum age, PhenoAge, and GrimAge) [25], and three summary-level aging-related traits (Aging-GIP1, socioeconomic traits-adjusted Aging-GIP1, and healthy aging) [25]. Aging-GIP1 is the first genetic principal component that captures both the length of life and age-related health status [27], which can be considered as a genetic representation of healthy longevity. It also shows the strongest genetic correlation with all other traits related to lifespan [25]. Therefore, we further used Aging-GIP1 as the primary aging-related trait to investigate CpG sites causal to the aging process. A genetic correlation analysis showed that all eight lifespan- and health-related traits are genetically correlated and clustered with each other, while the four epigenetic age measurements clustered with each other. GrimAge and PhenoAge showed significant genetic correlations with other health and lifespan-related traits, while Hannum age and Horvath age did not (Extended Data Fig. 1).

We then applied generalized inverse-variance weighted MR (gIVW) and MR-Egger (gEgger) on each exposure-outcome pair (Fig. 1b). We only included cis-meQTLs (meQTLs located within 2 MB of target CpG sites) in our analysis to avoid pleiotropic effects, as they are more likely to affect DNA methylation via direct mechanisms. To remove additional pleiotropic effects, we used the results of gEgger, whose estimate is robust to directional pleiotropic effects if the significant intercept is detected by gEgger regression ($P < 0.05$). After adjusting for multiple tests using Bonferroni correction, we discovered more than 6,000 CpG sites with significant causal effects on each trait, ranging from 5,507 (for GrimAge) to 8,341 (for self-rated health) (Fig. 1c).

Genetic colocalization is a Bayesian approach that estimates the probability (PP.H4) of overlapping genetic signals between molecular traits and outcome is due to both traits sharing a causal variant [28]. It is an important method to control false positive results from MR and filter out the MR signals purely driven by LD or pleiotropy. We then performed a pairwise conditional and colocalization (PWCoCo) analysis of all conditionally independent instruments against all conditionally independent association signals for the outcome phenotypes [29]. We used the conditional H4 threshold of 0.7 to identify colocalized signals and detected such signals for more than half of

the CpG sites identified by MR for each trait, ranging from 2,943 (for GrimAge) to 4,495 (for self-rated health).

Since we could only perform MR and colocalization analysis on 420,509 CpG sites, the role of unmeasured CpG sites on a tested trait could not be differentiated from the measured ones. To further validate whether the effect estimated by MR can be attributed to a single CpG site, we utilized the point mutation that naturally occurs on the causal CpG sites (C to A or C to T), also known as meSNP. For the human methylation array, nearly 10% of CpG sites have an meSNP available. We found that the meSNPs that occur at causal CpG sites have lower allele frequency in the population compared to noncausal CpG sites (Extended Data Fig. 2). Furthermore, the meSNPs were significantly depleted at causal CpG sites, suggesting that there is a negative selection against loss-of-function mutations at causal CpG sites (Extended Data Fig. 2). Among causal CpG sites with meSNPs available, we examined the correlation between the effects on the outcome trait estimated using a single meSNP and the effect estimated by MR. We observed a significant positive correlation between the two estimates (P = 1e-4, Pearson's R = 0.4, Extended Data Fig. 2). These results suggest that the causal effect estimated by MR can be partially attributed to a single CpG site, at least in the causal CpG sites with available meSNPs. Yet, considering many CpG sites do not have meSNPs available and the methylation level of individual CpG site tends to be highly correlated with neighboring CpG sites [30–32], we believe the causal CpG sites we identified also serve as tagging CpG sites for the causal regulatory region, and the causal effect size we estimated can be interpreted as the causal effect size of the tagged regulatory region.

Interestingly, the Spearman correlation of the estimated effect size of CpGs across twelve traits formed two distinct clusters, with the first cluster containing eight lifespan- and health-span-related traits, and the second all four epigenetic age measurements (Fig. 1d). This observation suggests that, although all these twelve traits are genetically correlated with each other, causal CpGs do not have proportional effect sizes – the CpGs with large effects on lifespan and healthspan do not have a proportional effect size on epigenetic age measurements and *vice versa*.

To prioritize CpG sites with the potential causal effect on Aging-GIP1, we first filtered MR signals based on the P value threshold after Bonferroni correction. The CpG sites were then ranked according to the magnitude of the causal effect, adjusted by the colocalization probability (PP.H4).

The top CpG sites whose methylation was observed to promote healthy longevity (Aging-GIP1) included cg12122041 at the *HTT* locus, which is associated with bone mineral density and age, cg02613937 at the *TOMM40* locus, which is associated with Alzheimer's disease and age, and cg19047158 at the non-coding region, which is associated with gestational age and rheumatoid arthritis. The top CpG sites whose methylation was found to inhibit healthy longevity included cg04977528 at the *HEYL* locus, which is associated with sex and age, cg06286026 at the *GRK4* locus (associated with age), cg27161488 at the *C4orf10* locus (associated with rheumatoid arthritis and age), and cg18744360 at the *MAD1L1* locus (associated with hypotensive disorder, Fig. 1e). Furthermore, cg19514613 at the *APOE* locus is also among the top sites that limit longevity. Genetic variants near *HTT* and *MAML3* were also shown to significantly affect lifespan in Finnish and Japanese cohorts in a previous study [33]. Both *TOMM40* and *APOE* are known to contribute to the risk of Alzheimer's disease and are associated with human lifespan [34,35]. Our results suggest that the known lifespan-related effect at these loci may be mediated by DNA methylation. Moreover, we also used adjusted Aging-GIP1, where the effects on human lifespan and healthspan that are correlated with socioeconomic status are removed. We showed that after adjusting for socioeconomic status, the CpG site with the top pro-longevity effect is cg06636172 at the *FOXO* locus, which is a major longevity locus [36,37].

To further understand the properties of the CpG sites identified as causal to each aging-related trait, we performed an enrichment analysis using 14 Roadmap annotations [38]. We found that the causal CpGs for most traits are enriched in promoters and enhancers while depleted in quiescent regions (Fig. 2a). Furthermore, the causal CpG sites were enriched in CpG shores (Extended Data Fig. 3). We observed that the causal CpG sites for Aging-GIP1 are significantly more evolutionally conserved compared to non-causal CpGs, based on both functional genomic conservation scores (Learning Evidence of Conservation from Integrated Functional genomic annotations, LECIF) and the phastCons/phyloP scores across 100 vertebrate genomes [39] (Fig. 2b, c, Extended Data Fig. 4). Moreover, the absolute value of the estimated causal effect sizes showed significant positive correlations between all three conservative scores. These results suggest that the CpG sites identified as causal for aging-related traits are more likely to be located in functional genomic elements and more evolutionarily conserved.

It is well known that DNA methylation status may affect the binding of transcription factors (TFs) [40]. To understand the relationship between causal CpG sites and TFs, we performed a transcription factor binding site enrichment analysis (Fig. 2d). The CpG sites causal to Aging-GIP1 were significantly enriched in the binding sites of 63 TFs, including *POLR2A*, *ZNF24*, *MYC*, and *HDAC1*; while depleted in the binding sites of 19 TFs, including *CTCF*, *CHD4*, and *BRD9* (Fig. 2d). In particular, *POLR2A* was among the top enriched TFs in 9 of 12 traits. POLR2A is the POLR2 subunit (RNA polymerase II), and previous research shows that epigenetic modifications can modulate its elongation and affect alternative splicing. Our results imply that this mechanism is potentially a major contributor that mediates the effects of DNA methylation on aging [10,11,41]. We further found that there were 3 TF-binding sites (*BRD4*, *CREB1*, and *E2F1*) enriched with CpG sites whose methylation levels promote healthy longevity (Aging-GIP1), and 4 TF-binding sites (*HDAC1*, *ZHX1*, *IKZF2*, and *IRF1*) enriched with CpG sites whose methylation levels decrease healthy longevity (Extended Data Fig. 5). *BRD4* contributes to cellular senescence and promotes inflammation [42]. Therefore, our findings suggest that higher DNA methylation at *BRD4* binding sites may inhibit the downstream effects of *BRD4* and promote healthy longevity. Similarly, previous studies showed that *CREB1* is related to type II diabetes and neurodegeneration [43], and mediates the effect of calorie restriction [44]. However, how DNA methylation may affect CREB1 binding is not well studied. Our data suggest that higher methylation at CREB1-binding sites may promote its longevity effects. *HDAC1* is a histone deacetylase, and its activity increases with aging and may promote age-related phenotypes [45,46]. *HDAC1* has been shown to specifically bind to methylated sites. Our data, therefore, support the hypothesis that *HDAC1* plays a damaging role during aging, as increased DNA methylation at *HDAC1* binding sites may causally inhibit healthy longevity.

We also checked the enrichment of causal CpG sites in phenome-wide EWAS signals obtained from the EWAS catalog [11]. The top enriched phenotypes included rheumatoid arthritis, HIV infection, nitrogen dioxide exposure, and maternal obesity (Fig. 2e). Interestingly, none of these conditions is primarily caused by aging. On the contrary, both rheumatoid arthritis and HIV infection are the conditions that have been suggested to accelerate aging and immunosenescence [41]. Additionally, maternal obesity is associated with accelerated metabolic aging in offspring [47], and nitrogen dioxide exposure is also shown to be associated with an increased risk of mortality [48]. Among the 12 traits tested, only the causal CpG sites for GrimAge and Hannum age (both are epigenetic

210 biomarker traits) were significantly enriched in the change of the CpG sites with aging, both epi-
211 genetic biomarker traits (Fig. 2e). Therefore, our results suggest that the causal CpG sites for aging
212 are enriched in conditions that cause accelerated aging, but not in conditions that are caused by
213 aging. This is consistent with the previous study, which suggests that differentially expressed genes
214 reflect disease-induced rather than disease-causing changes [49].

215 **MR on epigenetic age measurements successfully recovers clock sites as causal CpG sites**

216 For epigenetic age measurements, the causal CpG sites were the clock sites and the sites up-
217 stream of clock sites (Fig. 3a). To validate our EWMR approach for discovering causal CpG
218 sites, we used clock sites for each clock as ground truth and investigated whether MR could re-
219 cover the clock sites as causal CpG sites with the correct estimated effects.

220 We first examined the identified causal CpG sites for three epigenetic age measurements with the
221 clock models publicly available, namely HannumAge, HorvathAge, and PhenoAge [7]. We observed
222 that the causal CpGs identified by EWMR for each epigenetic age measurement were significantly
223 enriched with the corresponding clock sites (Fig. 3b; HannumAge P = 9.4e-9, HorvathAge P =
224 1.2e-12, PhenoAge P = 2.7e−6). Furthermore, EWMR predicted causal effect sizes of causal CpGs
225 with the correct direction and relative magnitude; as for the three epigenetic age measurements,
226 the estimated causal effect of MR showed a high and significant linear relationship with the actual
227 causal effect sizes denoted by the coefficients of the clock model (Fig. 3c-e). Notably, the enrich-
228 ment and correlation we described were also robust to the choice of threshold (Fig. 3b-e).

229 In MR studies, the P value is not a reliable ranking metric, as it is largely related to the number of
230 instruments available for the exposure traits [50]. As the epigenetic age GWAS provided a unique
231 opportunity where a part of the real causal CpG sites was already known, we applied four different
232 ranking metrics to identify an ideal ranking metric to rank causal CpG sites. We calculated the
233 area under the receiver operating curve (ROC, AUROC) using the clock sites as ground truth. The
234 AUROC measures the accuracy of binary classification, where an AUROC of 0.5 corresponds to
235 a random classification, and an AUROC of 1 corresponds to a perfect classification. Note that
236 since some causal CpGs are unknown (regulatory CpGs upstream to clock sites, Fig. 3a), the AU-
237 ROC we calculated underestimated the real accuracy. However, we found that when ranking with
238 PP-H4 weighted effect size, strikingly higher AUROCs were achieved compared to all other rank-
239 ing metrics (0.99 for HannumAge, 0.83 for HorvathAge, and 0.73 for PhenoAge, Fig. 3f, and

Extended Data Fig. 6). As far as we know, the colocalization probability-weighted effect size has never been used for ranking MR hits. Therefore, our findings provide novel metrics that could be reliably used to prioritize MR results of molecular traits and facilitate downstream analyses.

Existing epigenetic clocks are not enriched with CpG sites causal to aging

One open question for epigenetic clocks is whether their clock sites are causal to aging and age-related functional decline. To answer this question, we collected six epigenetic age models in humans with the clock sites publicly available, namely, the Zhang clock, PhenoAge, PedBE, HorvathAge, HannumAge, and Dunedin-PACE. We then performed an enrichment analysis of causal CpGs for all eight lifespan/healthspan-related traits for each clock. After correcting for multiple testing, none of the existing clocks showed significant enrichment for causal CpGs of any of the lifespan/healthspan-related traits (Fig. 3g). PhenoAge showed a nominal significant enrichment with CpGs causal to healthspan and healthy aging, but it was not robust to the choice of thresholds. This finding suggests that, although some clocks contain CpGs causal to aging (Table 1), they, by design, favor CpG sites with a higher correlation with age and thus are not enriched with causal CpGs.

In contrast, even though different clocks were trained on different datasets with different methods, the causal sites identified for one clock were usually also enriched with the clock sites for other clocks, suggesting that there is a subset of CpG sites that contribute to the epigenetic age estimate of all existing epigenetic clocks, which could potentially introduce systemic bias.

Integration of MR results and age-related changes reveals protective and deleterious epigenetic changes during aging

Another important question in epigenetic aging is the identity and number of epigenetic changes that (i) contribute to age-related damage and (ii) respond to it. We approached this question by integrating information on the causal effect and age-related change for each CpG. The protective or damaging nature of the age-related methylation change in each CpG is indicated by the product of the causal effect and age-related change ($b_{age} \times b_{MR}$, Fig. 4a). For example, if a higher methylation level of a certain CpG site leads to a longer lifespan or healthspan, then during aging, a decrease of the methylation level at that site would be considered as having a damaging effect, whereas an increased methylation level would be considered as having a protective effect.

The effect of DNA methylation estimated by MR is estimated through linear regression, which assumes that the relationship between DNA methylation level and lifespan-related outcome is linear. To annotate protective and damaging CpGs, it is important to understand whether the effect size of genetic instruments on DNA methylation levels is comparable with the effect of aging. If they are not at the same scale, the annotation could be inaccurate as age-related methylation changes may fall outside of the linear regions. We show that the effect of genetic instruments is comparable with the effect of aging by calculating the ratio between the effect of strongest meQTL and age-related methylation change (Extended Data Fig. 7). The median ratio is 21.8, suggesting that the median effect of genetic instruments is roughly equivalent to the effect of 21.8 years of aging.

Therefore, using the age-related blood DNA methylation change data estimated from 7,036 individuals (ages of 18 and 93 years, Generation Scotland cohort)[50], we separated the CpG sites causal to eight traits related to lifespan into four different categories: protective hypermethylation, deleterious hypermethylation, protective hypomethylation, and deleterious hypomethylation (Fig. 4b, Extended Data Fig. 8). Among the top 10 CpG sites whose methylation changes during aging have a relatively large impact on healthy longevity, we showed that six hypermethylated CpG sites during aging exhibit strong protective effects, including cg18327056, cg25700533, cg19095568, cg17227156, cg17113968, and cg07306253; while one hypomethylated CpG site (cg04977528) also has a protective effect. In contrast, 1 hypermethylated CpG sites (cg26669793) and 2 hypomethylated CpG sites (cg25903363 and cg26628907) show damaging effects (Fig. 4b).

Contradicting the popular notion that most age-related changes are bad for the organism, our findings revealed that, in terms of the number of CpGs, there was no enrichment for either protective or damaging methylation changes during aging (Extended Data Fig. 9). We also found that there was no significant correlation between the size of the causal effect and the magnitude of age-related changes (Fig. 4b, Extended Data Fig. 9), suggesting that CpG sites with a greater effect on healthy longevity do not necessarily change their level of methylation during aging. This result is consistent with our findings discussed above and explains the lack of enrichment of causal sites in existing epigenetic clocks.

As the product of the causal effect and age-related change ($b_{age} \times b_{MR}$) provides an estimate of the cumulative effect of age-related changes on aging-related phenotypes in a unit of time, we

calculated the cumulative effect of age-related changes on Aging-GIP1 (Fig. 4c). Importantly, we discovered that although the number of protective and damaging CpG sites was similar, the cumulative effect of combined age-related DNA methylation changes was detrimental to age-related phenotypes, consistent with the overall damaging nature of aging.

Algorithms for developing causality-informed epigenetic clocks

Although various existing epigenetic aging clock models can accurately predict the age of biological samples, they are purely based on correlation. This means that the reliability of existing clock models is highly dependent on the correlation structure of DNA methylation and phenotypes. This may result in unreliable estimates when extrapolating the model to predict the age of novel biological conditions (i.e., applying clocks to interventions that do not exist in the training population), as the correlation structure may be corrupted by the new intervention.

To overcome this problem, we developed novel epigenetic clocks that are based on causal CpG sites identified by EWMR (Fig. 5a). Specifically, we trained an elastic net model on whole blood methylation data from 2,664 individuals [51,52], using CpG sites identified as causal to Aging-GIP1 by EWMR (adjusted $P < 0.05$). In regular epigenetic clock models, the penalty weight is defined to be 1 for all CpG sites, which produces models that are purely based on correlation. Instead, we introduced a novel causality-informed elastic net model, where we assigned the feature-specific penalty factor based on the causality score for each CpG site (Method). The influence of the causality score on the feature-specific penalty factor is controlled by the causality factor τ, which is an adjustable parameter. If $\tau = 0$, the whole model is reduced to a regular elastic net regression, where the penalty factor equals one for all features. When τ becomes large, the model is more influenced by the causality score and tends to assign larger coefficients to the features with a higher causality score (Fig. 5A, Method).

Using this method, we trained the model to build the causality-informed epigenetic clock *CausAge* using 2,664 blood samples. We show that the model's accuracy decreased as the causality factor τ increased (Fig. 5b, c). This is because the causality factor τ controls the trade-off between the correlation and causality score-weighted penalty factor, and the causality score is not always correlated with the predictive power of age. For example, a CpG site with a high correlation with age may not be causal to aging, and *vice versa*. To balance clock accuracy and causality, we used the *CausAge* with the causality factor τ of 0.3 in the downstream analysis (Fig. 5c).

329 To separately measure adaptive and damaging DNA methylation changes during aging, we further
330 separated causal CpG sites into two groups based on the causal effect size from MR and the direc-
331 tion of age-related change (Fig. 4b). We then built *DamAge*, the damaging clock, which contains
332 only the damaging CpG sites, and *AdaptAge,* the protective clock, which contains only the adap-
333 tive/protective CpG sites (Fig. 5a). We show that both *DamAge* and *AdaptAge* can predict the age
334 of blood samples with similar accuracy. And similar to the *CausAge*, the accuracy of *DamAge* and
335 *AdaptAge* decreases as the causality factor τ increases (Fig. 5c).

336 **_DamAge_ and _AdaptAge_ clocks uncouple aging-related damage and adaptation**

337 By design, *AdaptAge* contains only the CpG sites that capture protective effects against aging.
338 Therefore, in theory, the subject predicted to be older by *AdaptAge* may be expected to accumu-
339 late more protective changes during aging. On the contrary, *DamAge* contains only the CpG sites
340 that exhibit damaging effects, which may be considered as a biomarker of age-related damage.
341 Therefore, we hypothesized that *DamAge* acceleration may be harmful and shorten life expec-
342 tancy, whereas *AdaptAge* acceleration would be protective or neutral, which may indicate
343 healthy longevity.

344 To test this hypothesis, we first analyzed the associations between human mortality and epigenetic
345 age acceleration quantified by causality-informed clocks using 4,651 individuals from the Fram-
346 ingham Heart Study, FHS offspring cohort (n = 2,544 Caucasians, 54% females) and Women's
347 Health Initiative cohort (WHI, n = 2107 postmenopausal women, Methods). Among the three cau-
348 sality-informed clocks, *DamAge* acceleration showed the strongest positive association on mortal-
349 ity and outperformed *CausAge* and Hannum clock, both of which exhibited a weaker positive as-
350 sociation with mortality (Fig. 5d, e). This finding supports the notion that age-related damage con-
351 tributes to the risk of mortality. In contrast, *AdaptAge* acceleration showed a significant negative
352 association with mortality, suggesting that protective adaptations during aging, measured by
353 *AdaptAge*, are associated with longer lifespan. In addition, epigenetic age accelerations measured
354 by *DamAge* and *AdaptAge* were only weakly associated (Pearson's R = 0.14, Extended Data Fig.
355 10). These findings highlight the importance of separating adaptive and damaging age-related
356 changes when building aging clock models.

357 Interestingly, although the clock accuracy monotonically decreased as the causality factor τ in-
358 creased, the association between mortality and epigenetic age acceleration did not follow the same

trend (Fig. 5e). Especially for *DamAge* and *CausAge*, the mortality association increased as the τ increased and peaked when τ was around 0.6. Also, *DamAge* consistently outperformed *CausAge* in predicting mortality risk, even though *CausAge* was more accurate in age prediction (Fig. 5b-e). This suggests that although the introduction of the causality score and separation of damaging CpGs may decrease the accuracy of the clock in terms of predicting chronological age, it improves the prediction of aging-related phenotypes.

Induced pluripotent stem cell (iPSC) reprogramming is one of the most robust rejuvenation models, which was shown to be able to strongly reverse the epigenetic age of cells [46]. We applied the causality-informed clock models to iPSC reprogramming [53]. For comparison, we also included three blood-based epigenetic models, namely Hannum clock, PhenoAge, and DunedinPace. The Hannum clock was trained on chronological age [54,55], PhenoAge was trained on the age adjusted by health-related phenotypes [56,57], and Dunedin-PACE was trained to predict the pace of aging [56]. Consistent with Hannum clock and PhenoAge, *DamAge* revealed that epigenetic age decreased during iPSC reprogramming, but with a stronger negative correlation with the time of reprogramming and higher statistical significance (Fig. 5f). This observation suggests that *DamAge* may better capture the damage-removal effect of iPSC reprogramming. On the contrary, *AdaptAge* increased significantly during the reprogramming process, suggesting that protective age-related changes do not capture the rejuvenation effect and that in fact cells may acquire even more protective changes during iPSC reprogramming.

Causality-informed epigenetic clocks capture damage and aging-related effects in the early stages

To further examine how *DamAge* and *AdaptAge* capture age-related damage and protective adaptations, respectively, we analyzed conditions that specifically promote age-related damage. Paraoxonase 1 (*PON1*) is one of most studied genes associated with cardiovascular disease, oxidative stress, inflammation, and healthy aging [58]. Specifically, *PON1* plays an important role in detoxifying organophosphorus compounds and removing harmful oxidized lipids [6]. The genetic variant of *PON1* (R192Q) significantly decreases PON1 activity and is known to be associated with an increased risk of cardiovascular disease and neurodegenerative diseases [59]. Interestingly, the *PON1* Q allele is significantly depleted in centenarians [60]. We analyzed the relationship between *PON1* activity and epigenetic age in 48 whole blood samples (Fig. 6a) [61]. *DamAge* shows

389 a significant negative correlation with *PON1* activity (R = -0.55, p = 0.0062), whereas *AdaptAge*
390 showed a significant positive correlation with *PON1* activity (R = 0.69, p = 0.0003). Again, this
391 association was not observed by other epigenetic clocks, except for Horvath age, but with a less
392 significant negative correlation.

393 By definition, causal epigenetic changes occur prior to downstream methylation changes and the
394 associated phenotypes (which are caused by upstream causal epigenetic changes). Therefore, we
395 hypothesized that the causality-informed clock models may be able to capture aging-related events
396 in the early stages, before downstream epigenetic mechanisms are triggered. Previous studies have
397 shown that anti-aging interventions during development could prolong lifespan and healthspan in
398 later life, including calorie restriction (CR) [62], and rapamycin treatment [63]. Small for gestational
399 age (SGA) is a condition defined as a birth weight less than the 10th percentile for gestational age
400 [64]. SGA is usually caused by nutritional deficiency during pregnancy; therefore, it can be consid-
401 ered a model of early life CR. We show that children with SGA have a significantly lower *DamAge*
402 and a higher *AdaptAge* than children with normal birth weight. This observation suggests that
403 *DamAge* and *AdaptAge* may be able to capture early-life CR effects, which are associated with
404 decreased damage accumulation and increased protective adaptations. These effects are not cap-
405 tured by the other epigenetic clocks tested. SGA is usually considered a pathological condition;
406 some studies suggest that this may be because early life benefits can be reversed in later life by
407 exposure to excessive nutrients [65]. The different roles of SGA in the early and late stages of life
408 may need to be further investigated in future studies.

409 In vitro fertilization (IVF) is a common method of treating infertility. Yet, previous studies have
410 shown that IVF may increase the risk of perinatal morbidity and mortality [66]. It has recently been
411 proposed that embryos undergo a rejuvenation event shortly after conception to remove age-related
412 damage [67,68]. Whether the *in vitro* environment of IVF affect this rejuvenation process is unknown.
413 We analyzed the DNA methylation data from neonatal blood spots of 137 newborns conceived
414 unassisted (NAT), through intrauterine insemination (IUI), or through IVF using fresh or cryo-
415 preserved (frozen) embryo transfer [69]. We found that IVF-conceived newborns using fresh or cry-
416 opreserved embryos have significantly higher *DamAge* acceleration and lower *AdaptAge* than
417 NAT-conceived newborns (Fig. 6b). On the other hand, IUI-conceived newborns show no

418 significant differences in both *DamAge* and *AdaptAge* compared to the control (Fig. 6b). This ef-
419 fect could not be observed by the other five epigenetic clocks tested, except for the Horvath age.

420 Genomic imprinting is an epigenetic mechanism that controls the expression of parent-of-origin-
421 dependent gene, which plays an important role in embryonic development and has a lifelong im-
422 pact on health [70]. Some imprinting genes are known to be associated with metabolic disorders and
423 aging (e.g., IGF2-H19) [71,72]. DNA methylation at imprinting loci is maintained during epigenetic
424 reprogramming in embryonic development, which coincides with the period of embryonic rejuve-
425 nation [67,68]. We analyzed the peripheral blood DNA methylation data from patients with single-
426 locus or Multi-loci imprinting disturbances (SLID or MLID), which is the condition of losing
427 methylation at single or multiple imprinting centers [73]. Similar to IVF, we found that patients with
428 imprinting disorders showed significantly higher *DamAge* and lower *AdaptAge* (Fig. 6b). To-
429 gether, these results suggest that *DamAge* and *AdaptAge* can serve as better biomarkers for events
430 affecting aging traits already during development.

431 Causality-informed clocks could also capture the aging-related effects of short-term interventions.
432 For example, we found that short-term treatment with cigarette smoke condensate in bronchial
433 epithelial cells significantly accelerated *DamAge* but did not affect other tested clocks (Fig. 6c).
434 Additionally, a 6-week omega-3 fatty acid supplementation in overweight subjects [74], which has
435 been shown to be protective against age-related cardiovascular diseases, significantly increased
436 *AdaptAge* and reduced *DamAge* (Fig. 6c). Together, our data demonstrate the importance of sep-
437 arating damage and adaptation when building biomarkers of aging and provide novel tools to quan-
438 tify aging and rejuvenation.

439 Discussion

440 Many existing epigenetic aging clock models accurately predict the age of samples [7], and there
441 are numerous CpG sites that are differentially methylated during aging [50]. DNA methylation lev-
442 els affect the structure of chromatin and the expression of neighboring genes [51,52], through which
443 they can causally affect aging-related phenotypes. A recent study also suggested that DNA meth-
444 ylation may play a causal role in the rejuvenation effect observed during iPSC reprogramming [46].
445 It is important to understand whether and which DNA methylation changes during aging cause
446 aging-related phenotypes. A previous transcriptome-wide MR study suggests that differentially

expressed genes in human diseases reflect mainly gene expression caused by disease rather than disease-causing genes [53]. Similarly, DNA methylation changes during aging may primarily reflect the downstream effects of aging phenotypes rather than causing them. Our EWMR findings further support this notion as we found no significant overlap between CpG sites causal to healthy longevity and those differentially methylated during aging.

MR is a powerful method to identify causal relationships between exposure traits and phenotypes [75]. However, it is limited by the availability of genetic instruments for the exposure traits. In our study, we utilized the DNA meQTLs of 420,509 CpG sites from the Illumina 450K methylation array as instrumental variables to infer their causal relationship with aging-related phenotypes. However, there are many unmeasured CpG sites across the genome, and the methylation patterns of nearby CpG sites are highly correlated [51]. Therefore, it is not possible to fully separate the causal effect of a single CpG and its neighbors. Analysis of point mutations at causal CpG sites (meSNPs) suggests that the epimutation of the single causal CpG site identified by MR may be sufficient to alter the phenotype (Extended Data Fig. 2). However, due to the lack of abundance of meSNPs on causal CpG sites, this hypothesis is difficult to test across all causal CpG sites we identified. Therefore, we tend to reach a more conservative conclusion and believe that the causal CpG sites identified in our study serve as tagging CpG sites for the causal regulatory regions in aging-related phenotypes. The genome-wide meQTL studies in the future may facilitate further refining of the causal effects of CpG sites at the base-pair resolution.

The genetic instruments of CpG sites were selected from the currently largest meQTL study in whole blood (GoDMC, 36 cohorts, including 27,750 European subjects). Therefore, the causal CpG sites we identified are primarily valid in blood. However, a previous study showed that up to 73% cis-meQTLs are shared across tissues [76]. This suggests that the identified causal CpG sites may also act in other tissues to affect lifespan and healthspan. Future large-scale meQTL studies across tissues may facilitate the identification of tissue-specific epigenetic effects on aging.

We found that TF-binding sites of *BRD4* and *CREB1* are enriched with CpG sites whose methylation levels promote healthy longevity, and TF-binding sites for *HDAC1* are enriched with CpG sites whose methylation levels decrease healthy longevity. *BRD4* contributes to cell senescence and promotes inflammation [42]. Therefore, our findings suggest that higher DNA methylation at *BRD4* binding sites may inhibit the downstream effects of *BRD4* and promote healthy longevity.

Similarly, previous studies showed that *CREB1* is related to type II diabetes and neurodegeneration [43], and mediates the effect of calorie restriction [44]. However, how DNA methylation may affect CREB1 binding is not well studied. Our data suggest that higher methylation at CREB1-binding sites may support its longevity effects. *HDAC1* is a histone deacetylase, and its activity increases with aging and may promote age-related phenotypes [45,46]. *HDAC1* has been shown to specifically bind to methylated sites. Our data, therefore, support the hypothesis that *HDAC1* plays a damaging role during aging, as increased DNA methylation at *HDAC1* binding sites may causally inhibit healthy longevity.

One general approach for developing anti-aging interventions is to identify molecular changes during aging and use these changes as targets to modulate the aging process [54,55]. A similar idea has also been applied to evaluate potential longevity interventions. However, this logic is intrinsically flawed, as correlation does not imply causation and age-related changes are not necessarily causal to age-associated declines. As living organisms are complex systems with various adaptive mechanisms, many molecular changes during aging are potentially neutral downstream effects of fundamental damaging changes or even adaptive mechanisms that protect against aging phenotypes. This notion is usually underappreciated as age-related changes are generally assumed to be damaging. As a result, adaptive mechanisms of aging are largely understudied. However, there is evidence to suggest that at least some age-related changes are protective against aging phenotypes.

An example of age-related protective changes is the Insulin and IGF-1 signaling (IIS) pathway. Attenuation of IIS signaling intensity through multiple genetic manipulations has been shown to consistently extend the lifespan of worms, flies, mice, and potentially humans [56,57]. This pathway also mediates pro-longevity effects of dietary restriction [56]. Growth hormone is produced by the anterior pituitary gland and can induce the production of IGF-1, thus increasing IIS signaling. Both growth hormone and IGF-1 levels decline during aging [58], which is considered to be a defensive response that extends lifespan [6]. Another example of an age-related adaptation is protein aggregation. It has been shown in *C. elegans* that the protein aggregation events are increased during aging. Although it may look like a result of losing proteostasis, it turns out to be a protective mechanism that drives aberrant proteins into insoluble aggregates to improve overall proteostasis, and has been observed in long-lived mutants [59]. Similar protective mechanisms are also observed in mouse nerves at the transcriptomic level [60].

Our results suggest that adaptive mechanisms at the epigenetic level are nearly as common as damaging changes and that simply following age-related changes in DNA methylation does not allow us to infer positive, neutral, or negative effects on age-related traits. However, the identified damaging and protective CpG sites are extremely useful both for understanding aging and quantifying it, and the same applies to rejuvenation. Together, the identified CpGs represent causal epigenetic changes, and their combined effect on health-related phenotypes is negative.

The framework we described for epigenetic changes in this study may be applied to any other age-related change, e.g., changes in the transcriptome, metabolome, and proteome. While all age-related features may be used to construct aging clocks, some of them are expected to be negative, some neutral, and some protective. Neither the direction nor the degree of change of age-related changes is important, and inferring the need to bring these changes to those observed in the young state as a way to rejuvenate an organism is equally incorrect. Instead, the focus should be on the causal effects of age-related changes, as well as on the direction of their effect.

The causal epigenetic clock models, *CausAge*, *AdaptAge*, and *DamAge*, could help separate protective changes from damaging events. We also showed that by preselecting the CpG sites that show protective adaptation during aging, it is possible to build an aging clock showing an inverse relationship with mortality. Specifically, subjects with elevated protective adaptation are predicted to be age-accelerated by *AdaptAge* and have a lower risk of mortality (Fig. 5c). Similarly, *AdaptAge* shows an inverse relationship with rejuvenation (e.g., iPSC reprogramming) and aging acceleration. Note that both *DamAge* and *AdaptAge* show similar accuracy in predicting chronological age, but their delta-age term shows an opposite biological meaning. This finding suggests that we should reconsider the way we interpret "epigenetic age acceleration" in clinical settings, especially for the clocks that are trained in a regular way, which contain a mixture of adaptative and damaging CpG sites. Together, our finding highlights the importance of pre-selecting deleterious CpG sites when building aging clock models, and our causality-informed clock models provide novel insights into the aging mechanisms and testing interventions that delay aging and reverse biological age.

Acknowledgments

We thank the DNA Methylation Consortium (GoDMC) for releasing the summary statistics of meQTLs. We also thank Csaba Kerepesi, Marco Mariotti, Daniel L. McCartney, and Riccardo E. Marioni for help and advice during the initial stage of the study. Supported by NIA, Impetus grants and the Michael Antonov Foundation.

Author contributions

K.Y. initiated the study; K.Y. collected and analyzed the data; V.N.G. supervised the study. K.Y., H.L., and A.T. performed data analyses; All authors contributed to paper writing.

Competing interest statement

The authors declare no competing financial interests.

Data availability statement

Data generated in this study will be publicly available upon publication.

Code availability statement

Code used will be publicly available upon publication.

References

1. Chauhan, A. *et al.* Systems biology approaches in aging research. *Interdiscip Top Gerontol* **40**, 155–76 (2015).
2. Sen, P., Shah, P. P., Nativio, R. & Berger, S. L. Epigenetic Mechanisms of Longevity and Aging. *Cell* **166**, 822–839 (2016).
3. Guibert, S. & Weber, M. Functions of DNA methylation and hydroxymethylation in mammalian development. *Curr Top Dev Biol* **104**, 47–83 (2013).
4. Jones, P. A. Functions of DNA methylation: islands, start sites, gene bodies and beyond. *Nat. Rev. Genet.* **13**, 484–492 (2012).

557 5. Kane, A. E. & Sinclair, D. A. Epigenetic changes during aging and their reprogramming potential.
558 *Crit Rev Biochem Mol Biol* **54**, 61–83 (2019).
559 6. López-Otín, C., Blasco, M. A., Partridge, L., Serrano, M. & Kroemer, G. The Hallmarks of Aging.
560 *Cell* **153**, 1194–1217 (2013).
561 7. Bell, C. G. *et al.* DNA methylation aging clocks: challenges and recommendations. *Genome Biol* **20**,
562 249 (2019).
563 8. A. Reynolds, C. *et al.* A decade of epigenetic change in aging twins: Genetic and environmental con-
564 tributions to longitudinal DNA methylation. *Aging Cell* **19**, (2020).
565 9. Field, A. E. *et al.* DNA Methylation Clocks in Aging: Categories, Causes, and Consequences. *Mol*
566 *Cell* **71**, 882–895 (2018).
567 10. Horvath, S. DNA methylation age of human tissues and cell types. *Genome Biol.* **14**, R115 (2013).
568 11. Hannum, G. *et al.* Genome-wide methylation profiles reveal quantitative views of human aging rates.
569 *Mol. Cell* **49**, 359–367 (2013).
570 12. Quach, A. *et al.* Epigenetic clock analysis of diet, exercise, education, and lifestyle factors. *Aging* **9**,
571 419–446 (2017).
572 13. Rutledge, J., Oh, H. & Wyss-Coray, T. Measuring biological age using omics data. *Nat. Rev. Genet.*
573 (2022) doi:10.1038/s41576-022-00511-7.
574 14. Kapur, K. Chapter 14 - Principles of Biostatistics. in *Clinical and Translational Science (Second Edi-*
575 *tion)* (eds. Robertson, D. & Williams, G. H.) 243–260 (Academic Press, 2017). doi:10.1016/B978-0-
576 12-802101-9.00014-4.
577 15. Davey Smith, G. & Hemani, G. Mendelian randomization: genetic anchors for causal inference in ep-
578 idemiological studies. *Hum Mol Genet* **23**, R89-98 (2014).
579 16. Evans, D. M. & Davey Smith, G. Mendelian Randomization: New Applications in the Coming Age
580 of Hypothesis-Free Causality. *Annu Rev Genomics Hum Genet* **16**, 327–50 (2015).
581 17. Neumeyer, S., Hemani, G. & Zeggini, E. Strengthening Causal Inference for Complex Disease Using
582 Molecular Quantitative Trait Loci. *Trends Mol Med* **26**, 232–241 (2020).

583 18. Võsa, U. *et al.* Large-scale cis- and trans-eQTL analyses identify thousands of genetic loci and poly-
584 genic scores that regulate blood gene expression. *Nat. Genet.* **53**, 1300–1310 (2021).
585 19. Garrido-Martín, D., Borsari, B., Calvo, M., Reverter, F. & Guigó, R. Identification and analysis of
586 splicing quantitative trait loci across multiple tissues in the human genome. *Nat. Commun.* **12**, 727
587 (2021).
588 20. He, B., Shi, J., Wang, X., Jiang, H. & Zhu, H.-J. Genome-wide pQTL analysis of protein expression
589 regulatory networks in the human liver. *BMC Biol.* **18**, 97 (2020).
590 21. Kraus, W. E. *et al.* Metabolomic Quantitative Trait Loci (mQTL) Mapping Implicates the Ubiquitin
591 Proteasome System in Cardiovascular Disease Pathogenesis. *PLoS Genet* **11**, e1005553 (2015).
592 22. Huan, T. *et al.* Genome-wide identification of DNA methylation QTLs in whole blood highlights
593 pathways for cardiovascular disease. *Nat Commun* **10**, 4267 (2019).
594 23. Richardson, T. G. *et al.* Systematic Mendelian randomization framework elucidates hundreds of CpG
595 sites which may mediate the influence of genetic variants on disease. *Hum. Mol. Genet.* **27**, 3293–
596 3304 (2018).
597 24. McCartney, D. L. *et al.* Genome-wide association studies identify 137 genetic loci for DNA methyla-
598 tion biomarkers of aging. *Genome Biol.* **22**, 194 (2021).
599 25. Timmers, P. R. H. J. *et al.* Mendelian randomization of genetically independent aging phenotypes
600 identifies LPA and VCAM1 as biological targets for human aging. *Nat. Aging* **2**, 19–30 (2022).
601 26. Timmers, P., Wilson, J. F., Joshi, P. K. & Deelen, J. Multivariate genomic scan implicates novel loci
602 and haem metabolism in human ageing. *Nat Commun* **11**, 3570 (2020).
603 27. Kundaje, A. *et al.* Integrative analysis of 111 reference human epigenomes. *Nature* **518**, 317–330
604 (2015).
605 28. Wallace, C. Eliciting priors and relaxing the single causal variant assumption in colocalisation anal-
606 yses. *PLOS Genet.* **16**, e1008720 (2020).

607 29. Robinson, J. W. *et al.* An efficient and robust tool for colocalisation: Pair-wise Conditional and Colo-
608 calisation (PWCoCo). 2022.08.08.503158 Preprint at https://doi.org/10.1101/2022.08.08.503158
609 (2022).
610 30. Timmers, P. R. *et al.* Genomics of 1 million parent lifespans implicates novel pathways and common
611 diseases and distinguishes survival chances. *eLife* **8**, e39856 (2019).
612 31. Shao, Y. *et al.* DNA methylation of TOMM40-APOE-APOC2 in Alzheimer's disease. *J. Hum.*
613 *Genet.* **63**, 459–471 (2018).
614 32. Goh, L. K. *et al.* TOMM40 alterations in Alzheimer's disease over a 2-year follow-up period. *J. Alz-*
615 *heimers Dis. JAD* **44**, 57–61 (2015).
616 33. Hu, S. *et al.* DNA methylation presents distinct binding sites for human transcription factors. *eLife* **2**,
617 e00726 (2013).
618 34. González-Rodríguez, P., Klionsky, D. J. & Joseph, B. Autophagy regulation by RNA alternative
619 splicing and implications in human diseases. *Nat. Commun.* **13**, 2735 (2022).
620 35. Saldi, T., Cortazar, M. A., Sheridan, R. M. & Bentley, D. L. Coupling of RNA Polymerase II Tran-
621 scription Elongation with Pre-mRNA Splicing. *J. Mol. Biol.* **428**, 2623–2635 (2016).
622 36. Hua, T. *et al.* BRD4 Inhibition Attenuates Inflammatory Pain by Ameliorating NLRP3 Inflam-
623 masome-Induced Pyroptosis. *Front. Immunol.* **13**, 837977 (2022).
624 37. Wang, H. *et al.* BRD4 contributes to LPS-induced macrophage senescence and promotes progression
625 of atherosclerosis-associated lipid uptake. *Aging* **12**, 9240–9259 (2020).
626 38. Herzig, S. *et al.* CREB regulates hepatic gluconeogenesis through the coactivator PGC-1. *Nature*
627 **413**, 179–183 (2001).
628 39. Fusco, S. *et al.* A role for neuronal cAMP responsive-element binding (CREB)-1 in brain responses
629 to calorie restriction. *Proc. Natl. Acad. Sci.* **109**, 621–626 (2012).
630 40. Willis-Martinez, D., Richards, H. W., Timchenko, N. A. & Medrano, E. E. Role of HDAC1 in senes-
631 cence, aging, and cancer. *Exp. Gerontol.* **45**, 279–285 (2010).

632 41. Levine, M. E. *et al.* An epigenetic biomarker of aging for lifespan and healthspan. *Aging* **10**, 573–591
633 (2018).
634 42. Burgess, S., Zuber, V., Valdes-Marquez, E., Sun, B. B. & Hopewell, J. C. Mendelian randomization
635 with fine-mapped genetic data: Choosing from large numbers of correlated instrumental variables.
636 *Genet. Epidemiol.* **41**, 714–725 (2017).
637 43. Lehne, B. *et al.* A coherent approach for analysis of the Illumina HumanMethylation450 BeadChip
638 improves data quality and performance in epigenome-wide association studies. *Genome Biol.* **16**, 37
639 (2015).
640 44. Ohnuki, M. *et al.* Dynamic regulation of human endogenous retroviruses mediates factor-induced re-
641 programming and differentiation potential. *Proc. Natl. Acad. Sci. U. S. A.* **111**, 12426–12431 (2014).
642 45. Rando, T. A. & Chang, H. Y. Aging, Rejuvenation, and Epigenetic Reprogramming: Resetting the
643 Aging Clock. *Cell* **148**, 46–57 (2012).
644 46. Lu, Y. *et al.* Reprogramming to recover youthful epigenetic information and restore vision. *Nature*
645 **588**, 124–129 (2020).
646 47. Belsky, D. W. *et al.* Quantification of the pace of biological aging in humans through a blood test, the
647 DunedinPoAm DNA methylation algorithm. *eLife* **9**, e54870 (2020).
648 48. Stewart, E. A. *et al.* Uterine fibroids. *Nat. Rev. Dis. Primer* **2**, 16043 (2016).
649 49. George, J. W. *et al.* Integrated Epigenome, Exome, and Transcriptome Analyses Reveal Molecular
650 Subtypes and Homeotic Transformation in Uterine Fibroids. *Cell Rep.* **29**, 4069-4085.e6 (2019).
651 50. McCartney, D. L. *et al.* An epigenome-wide association study of sex-specific chronological ageing.
652 *Genome Med.* **12**, 1 (2019).
653 51. Huh, I., Zeng, J., Park, T. & Yi, S. V. DNA methylation and transcriptional noise. *Epigenetics Chro-*
654 *matin* **6**, 9 (2013).
655 52. Kim, S., Park, H. J., Cui, X. & Zhi, D. Collective effects of long-range DNA methylations predict
656 gene expressions and estimate phenotypes in cancer. *Sci. Rep.* **10**, 1–12 (2020).

657 53. Porcu, E. *et al.* Differentially expressed genes reflect disease-induced rather than disease-causing
658 changes in the transcriptome. *Nat. Commun.* **12**, 5647 (2021).
659 54. Tollefsbol, T. O. Techniques for Analysis of Biological Aging. *Methods Mol. Biol. Clifton NJ* **371**,
660 1–7 (2007).
661 55. Tosato, M., Zamboni, V., Ferrini, A. & Cesari, M. The aging process and potential interventions to
662 extend life expectancy. *Clin. Interv. Aging* **2**, 401–412 (2007).
663 56. Fontana, L., Partridge, L. & Longo, V. D. Extending healthy life span--from yeast to humans. *Science*
664 **328**, 321–6 (2010).
665 57. Milman, S. *et al.* Low insulin-like growth factor-1 level predicts survival in humans with exceptional
666 longevity. *Aging Cell* **13**, 769–771 (2014).
667 58. Schumacher, B. *et al.* Delayed and Accelerated Aging Share Common Longevity Assurance Mecha-
668 nisms. *PLOS Genet.* **4**, e1000161 (2008).
669 59. Walther, D. M. *et al.* Widespread Proteome Remodeling and Aggregation in Aging C. elegans. *Cell*
670 **161**, 919–932 (2015).
671 60. Goto, K. *et al.* Protective mechanism against age-associated changes in the peripheral nerves. *Life*
672 *Sci.* **253**, 117744 (2020).
673 61. Declerck, K. *et al.* Interaction between prenatal pesticide exposure and a common polymorphism in
674 the PON1 gene on DNA methylation in genes associated with cardio-metabolic disease risk-an ex-
675 ploratory study. *Clin. Epigenetics* **9**, 35 (2017).
676 62. Sun, L., Sadighi Akha, A. A., Miller, R. A. & Harper, J. M. Life-span extension in mice by prewean-
677 ing food restriction and by methionine restriction in middle age. *J. Gerontol. A. Biol. Sci. Med. Sci.*
678 **64**, 711–722 (2009).
679 63. Shindyapina, A. V. *et al.* Rapamycin treatment during development extends life span and health span
680 of male mice and Daphnia magna. *Sci. Adv.* **8**, eabo5482 (2022).
681 64. Osuchukwu, O. O. & Reed, D. J. Small for Gestational Age. in *StatPearls* (StatPearls Publishing,
682 2022).

683 65. Ribeiro, A. M., Lima, M. de C., de Lira, P. I. C. & da Silva, G. A. P. Low birth weight and obesity:
684 causal or casual casual association? *Rev. Paul. Pediatr.* **33**, 340–348 (2015).
685 66. Sabban, H., Zakhari, A., Patenaude, V., Tulandi, T. & Abenhaim, H. A. Obstetrical and perinatal
686 morbidity and mortality among in-vitro fertilization pregnancies: a population-based study. *Arch. Gy-*
687 *necol. Obstet.* **296**, 107–113 (2017).
688 67. Gladyshev, V. N. The Ground Zero of Organismal Life and Aging. *Trends Mol. Med.* **27**, 11–19
689 (2021).
690 68. Kerepesi, C., Zhang, B., Lee, S.-G., Trapp, A. & Gladyshev, V. N. Epigenetic clocks reveal a rejuve-
691 nation event during embryogenesis followed by aging. *Sci. Adv.* **7**, eabg6082 (2021).
692 69. Estill, M. S. *et al.* Assisted reproductive technology alters deoxyribonucleic acid methylation profiles
693 in bloodspots of newborn infants. *Fertil. Steril.* **106**, 629-639.e10 (2016).
694 70. Monk, D., Mackay, D. J. G., Eggermann, T., Maher, E. R. & Riccio, A. Genomic imprinting disor-
695 ders: lessons on how genome, epigenome and environment interact. *Nat. Rev. Genet.* **20**, 235–248
696 (2019).
697 71. Ratajczak, M. Z. Igf2-H19, an imprinted tandem gene, is an important regulator of embryonic devel-
698 opment, a guardian of proliferation of adult pluripotent stem cells, a regulator of longevity, and a
699 'passkey' to cancerogenesis. *Folia Histochem. Cytobiol.* **50**, 171–179 (2012).
700 72. Butler, M. G. Genomic imprinting disorders in humans: a mini-review. *J. Assist. Reprod. Genet.* **26**,
701 477 (2009).
702 73. Bens, S. *et al.* Phenotypic spectrum and extent of DNA methylation defects associated with multi-
703 locus imprinting disturbances. *Epigenomics* **8**, 801–816 (2016).
704 74. Tremblay, B. L. *et al.* Epigenetic changes in blood leukocytes following an omega-3 fatty acid sup-
705 plementation. *Clin. Epigenetics* **9**, 43 (2017).
706 75. Emdin, C. A., Khera, A. V. & Kathiresan, S. Mendelian Randomization. *JAMA* **318**, 1925–1926
707 (2017).

708 76. Lin, D. *et al.* Characterization of cross-tissue genetic-epigenetic effects and their patterns in schizo-
709 phrenia. *Genome Med.* **10**, 13 (2018).

710

711 ## Figure legends

712 **Fig. 1. Epigenome-wide Mendelian Randomization on various aging-related phenotypes. a.**
713 Schematic diagram shows the principle of MR using meQTLs as exposures and aging-related
714 traits as outcomes to identify causal CpG sites. **b.** The flow chart shows the procedure for epige-
715 nome-wide MR and sensitivity analysis. **c.** Number of significant causal CpG sites identified for
716 each trait after adjusting for multiple tests using the Bonferroni correction. The darker regions of
717 the bars indicate the number of causal CpG sites supported by the colocalization analysis with
718 conditional PP-H4 > 0.7. **d.** Spearman correlation of the estimated causal effects of CpGs in
719 twelve traits. Only CpGs with significant MR signals across at least six traits are included in the
720 analysis. The color scheme corresponds to the Spearman correlation coefficient, * adjusted $P <$
721 0.05, ** adjusted $P < 0.01$, *** adjusted $P < 0.001$. **e.** The modified Mississippi plot shows sig-
722 nificant MR signals for Aging-GIP1. The X-axis corresponds to the genomic positions of CpG
723 sites; Y-axis represents the size of the causal effect adjusted by colocalization probability (PP-
724 H4). CpG sites with top adjusted causal effects are annotated with the name and nearest gene.
725 Only CpG sites with adjusted $P < 0.05$ are included in the plot.

726 **Fig. 2. CpG sites causal to aging are enriched in specific genetic regulatory regions. a.** The
727 bar plot shows the enrichment of causal CpG sites in 14 Roadmap genomic annotations. The Y
728 axis shows -log10 (FDR) based on Fisher's exact test, signed by log2 (Odds ratio). Causal CpG
729 sites identified for different traits are annotated with different colors. Two dotted horizontal lines
730 show the FDR threshold of 0.05. TssA, active transcription start site. Prom, upstream/downstream
731 TSS promoter. Tx, actively transcribed state. TxWk, weak transcription. TxEn, transcribed and
732 regulatory Prom/Enh. EnhA, active enhancer. EnhW, weak enhancer. DNase, primary DNase.
733 ZNF/Rpts, state associated with zinc finger protein genes. Het, constitutive heterochromatin.
734 PromP, Poised promoter. PromBiv, bivalent regulatory states. ReprPC, repressed polycomb states.
735 Quies, quiescent state. **b, c.** The box plot shows the distribution of conservation scores in causal
736 and non-causal CpG sites. The conservation scores are obtained by Learning Evidence of Conser-
737 vation from Integrated Functional genomic annotations (LECIF, **b**) and phastCons (**c**). * $P < 0.05$,
738 ** $P < 0.01$, *** $P < 0.001$, **** $P < 0.0001$. **d, e.** Enrichment of causal CpG sites for 12 aging-
739 related traits against transcription-factor-binding sites (**d**) and EWAS hits (**e**). Each horizontal bar

740 represents an enriched term. The X-axis shows the -log10(*P*-value), signed by log2 (Odds ratio).
741 The top 10 enriched terms that passed the FDR threshold of 0.05 for each direction are annotated.

742 **Fig. 3. MR on epigenetic age successfully recovers clock sites as causal CpG sites. a.** For epi-
743 genetic age measurements, true causal sites are the clock sites and the sites upstream of clock sites.
744 We used these traits as a positive control to validate the MR approach for identifying causal CpGs.
745 **b**. The forest plot shows the enrichment of clock sites for each model in causal CpG sites identified
746 by MR for each trait. The X-axis shows the log2(Odds Ratio). *P*-values calculated by Fisher's
747 exact test are annotated. Error bars show 95% confidence intervals. Different colors represent dif-
748 ferent thresholds for causal CpGs. **c-e.** Correlation between ground truth causal effects (clock co-
749 efficients, X-axis) and causal effects estimated by MR (Y-axis) for Hannum age (**c**), Horvath age
750 (d) and PhenoAge (**e**). Different colors represent different thresholds for causal CpGs. Pearson's
751 correlation coefficients and *P*-values are annotated. **f.** The receiver operating characteristic (ROC)
752 curves show the sensitivity (Y-axis) and the 1-specificity (X-axis) of MR in identifying causal
753 CpG sites for clock traits, with the area under the ROC curve (AUC) annotated. **g.** The forest plot
754 shows the enrichment of clock sites for six aging clock models in causal CpG sites identified by
755 MR for each trait. The X-axis shows the log2(Odds Ratio). *P*-values calculated by Fisher's exact
756 test are annotated if $P < 0.05$. Error bars show 95% confidence intervals. Different colors represent
757 the different thresholds for causal CpGs.

758 **Fig. 4. Integration of causal information and age-related changes to separate protective and**
759 **damaging epigenetic changes. a.** Schematic diagram showing the method to identify protective
760 and damaging epigenetic changes by integrating MR results and age-related differential methyla-
761 tion. **b.** Relationship between MR-estimated causal effects (X-axis) and age-related methylation
762 change (Y-axis) for each significant causal CpG identified in Aging-GIP1. The color scheme high-
763 lights the expected impact of age-related methylation change on aging. Error bars show the stand-
764 ard error of *b*. The size reflects the PP-H4. Only CpG sites with adjusted *P*-values < 0.05 and
765 relative PP-H4 > 0.7 are plotted. The CpG sites with the top 10 largest effect sizes are annotated.
766 **c.** Area plots show the total cumulative effect of changes in DNA methylation on Aging-GIP1.
767 The X-axis shows the rank of the CpG sites based on the impact of age-related changes
768 ($b_{age:CpG} \times b_{CpG:MR}$). The Y-axis and the color scheme show the cumulative sum of impacts.

Fig. 5. Construction and application of causality-informed epigenetic clocks. a. Schematic diagram shows the procedure of constructing causality-informed epigenetic clocks. **b.** Scatter plots show the accuracy of causal clocks on the test set. The X-axis shows the real age of each sample, and the Y-axis shows the predicted age of the same sample based on each clock model. Median absolute error (MAE) and Pearson's R are annotated. **c.** Line plot showing the relationship between causality factor (τ) and clock accuracy measured by MAE and Pearson's R. **d.** The forest plot shows the Log2 hazard ratio of mortality risk for every 10-year increase in age for each clock model. *The P values* are annotated if $P < 0.05$. The error bars show the standard error of the log2 hazard ratio. **e.** The line plot shows the relationship between the causality factor (τ) and -log10(p) for the association with mortality risk (signed by log2(hazard ratio)). The yellow dashed line shows the *P* threshold of 0.05. The orange dotted line shows the significance score for Hannum age acceleration **f.** The scatter plots show the application of causal clocks and three other blood-based clocks to iPSC reprogramming. The X-axis shows the days after initiating reprogramming. Pearson's R and *P* values are annotated.

Fig. 6. Causality-informed epigenetic clocks capture aging-related effects in the early stages. a. Scatter plots show the correlation between epigenetic age and blood *PON1* activity. Epigenetic age prediction is rescaled to a 0-1 scale for better comparison. The color shows the *PON1* genotype in subjects. Linear regression is performed, and Pearson's R and *P* values are annotated. **b.** Box plots show the association between the epigenetic age and the conditions at early developmental stages, including the small for gestational age (SGA), the in vitro fertilization, and imprinting disturbances. IUI, intrauterine insemination; IVF, in vitro fertilization; SLID, single locus imprinting disorder; MLID, multiple loci imprinting disorder. **c.** Box plots show the association between the epigenetic age and short-term treatments, including the 15 months of cigarette smoke condensate (CSC) treatment and the 6-week supplementation of omega-3 fatty acid supplementation in overweight subjects. For all box plots, the significant pairs based on the two-tail t-test are annotated with stars, and the *P* values from the ANOVA test are annotated. * $P < 0.05$, ** $P < 0.01$, *** $P < 0.001$, **** $P < 0.0001$.

797 **Table 1.** Causal CpG sites in existing epigenetic clocks

	Position	Weight	outcome	Beta	SE	P	H4	role
HorvathAge (353)	cg06557358	-0.14	Overall_health_rating	-0.04	0.008	1.96E-07	0.89	Protective
	cg09509673	0.01	Healthy-aging	0.02	0.003	3.86E-13	0.85	Protective
	cg09509673	0.01	Lifespan	0.05	0.006	9.92E-20	0.83	Protective
	cg11299964	-0.16	Aging-GIP1	0.08	0.012	5.42E-12	0.86	Deleterious
	cg16744741	-0.35	Aging-GIP1	0.09	0.017	1.86E-08	0.89	Deleterious
	cg16744741	-0.35	Overall_health_rating	0.06	0.008	6.10E-14	0.86	Deleterious
PhenoAge (513)	cg05087948	-6.99	Aging-GIP1-adj	-0.08	0.013	7.30E-10	1.00	Protective
	cg21926612	-2.15	Overall_health_rating	0.01	0.002	3.27E-11	0.94	Deleterious
	cg11896923	-1.38	Healthspan	0.17	0.024	4.64E-12	0.90	Deleterious
	cg11896923	-1.38	Healthy-aging	0.05	0.008	5.63E-10	0.86	Deleterious
	cg00862290	-0.23	Healthy-aging	0.00	0.001	1.28E-08	0.85	Protective
	cg00862290	-0.23	Lifespan	-0.02	0.003	0	0.94	Protective
Zhang (514)	cg24987259	-1.33	Overall_health_rating	-0.04	0.007	8.25E-09	0.95	Protective
	cg05310309	0.18	Aging-GIP1	0.03	0.003	1.13E-32	0.96	Protective
	cg05310309	0.18	Overall_health_rating	0.01	0.002	2.64E-12	0.92	Protective
	cg06672696	0.02	Frailty-index	0.05	0.010	1.74E-07	0.82	Protective
PedBE (94)	cg04221461	0.03	Frailty-index	0.04	0.008	1.25E-07	0.95	Protective
	cg19381811	-0.08	Aging-GIP1	-0.04	0.004	3.26E-21	0.929544	Protective
	cg19381811	-0.08	Overall_health_rating	-0.03	0.002	8.80E-37	0.955032	Protective

Fig. 1

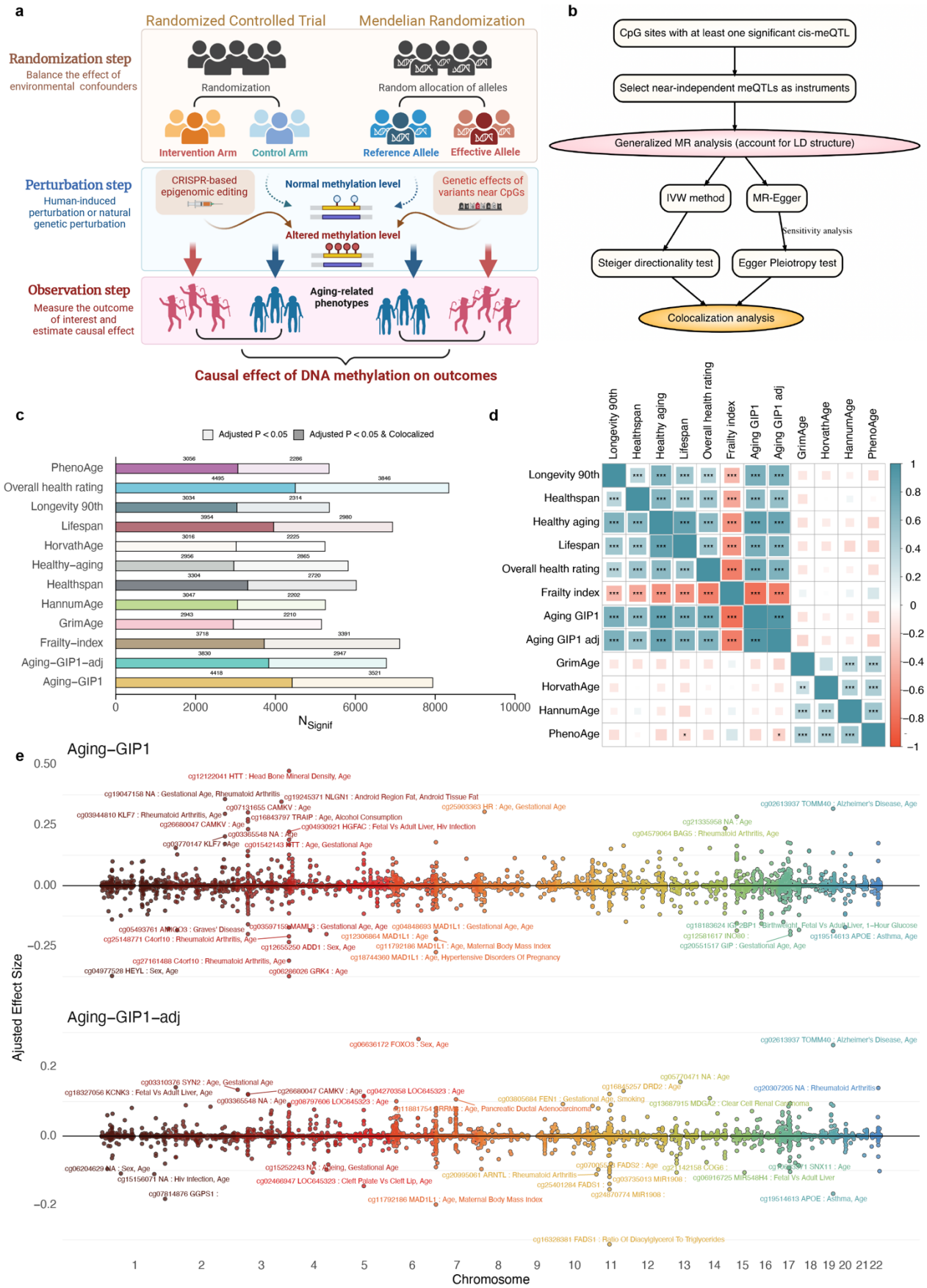
a
Randomized Controlled Trial
Mendelian Randomization
Randomization step
Balance the effect of environmental confounders
Randomization
Random allocation of alleles
Intervention Arm
Control Arm
Reference Allele
Effective Allele
Perturbation step
Human-induced perturbation or natural genetic perturbation
CRISPR-based epigenomic editing
Normal methylation level
Genetic effects of variants near CpGs
Altered methylation level
Observation step
Measure the outcome of interest and estimate causal effect
Aging-related phenotypes
Causal effect of DNA methylation on outcomes
b
CpG sites with at least one significant cis-meQTL
Select near-independent meQTLs as instruments
Generalized MR analysis (account for LD structure)
IVW method
MR-Egger
Sensitivity analysis
Steiger directionality test
Egger Pleiotropy test
Colocalization analysis
c
Adjusted P < 0.05
Adjusted P < 0.05 & Colocalized
PhenoAge
Overall health rating
Longevity 90th
Lifespan
HorvathAge
Healthy–aging
Healthspan
HannumAge
GrimAge
Frailty–index
Aging–GIP1–adj
Aging–GIP1
N_Signif
d
Longevity 90th
Healthspan
Healthy aging
Lifespan
Overall health rating
Frailty index
Aging GIP1
Aging GIP1 adj
GrimAge
HorvathAge
HannumAge
PhenoAge
e
Aging–GIP1
Aging–GIP1–adj
Ajusted Effect Size
Chromosome

Fig. 2

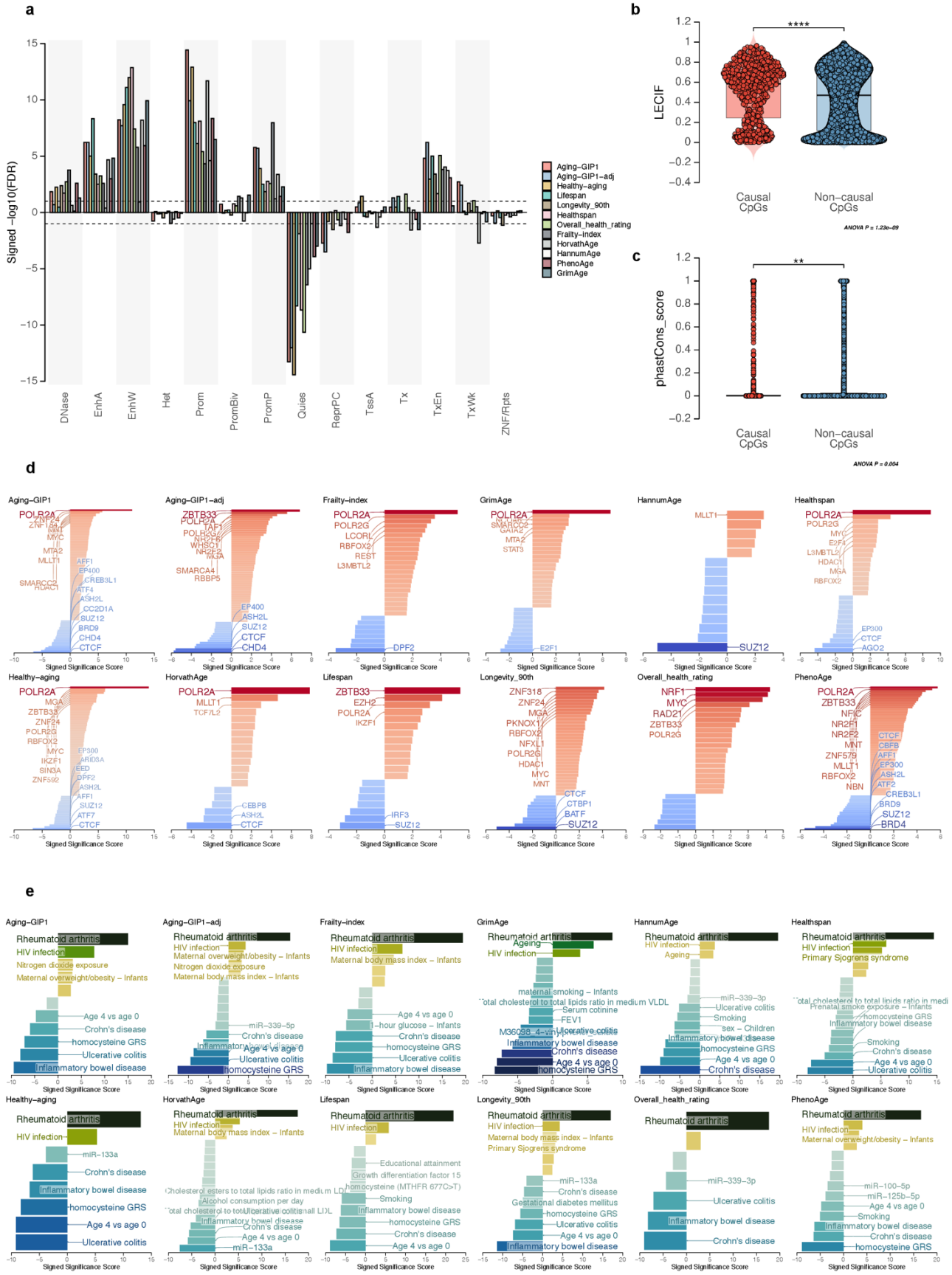
a
Signed −log10(FDR)
DNase
EnhA
EnhW
Het
Prom
PromBiv
PromP
Quies
ReprPC
TssA
Tx
TxEn
TxWk
ZNF/Rpts
Aging−GIP1
Aging−GIP1−adj
Healthy−aging
Lifespan
Longevity_90th
Healthspan
Overall_health_rating
Frailty−index
HorvathAge
HannumAge
PhenoAge
GrimAge
b
LECIF
Causal CpGs
Non−causal CpGs
ANOVA P = 1.23e−09
c
phastCons_score
Causal CpGs
Non−causal CpGs
ANOVA P = 0.004
d
Signed Significance Score
e
Signed Significance Score

801 **Fig. 3**

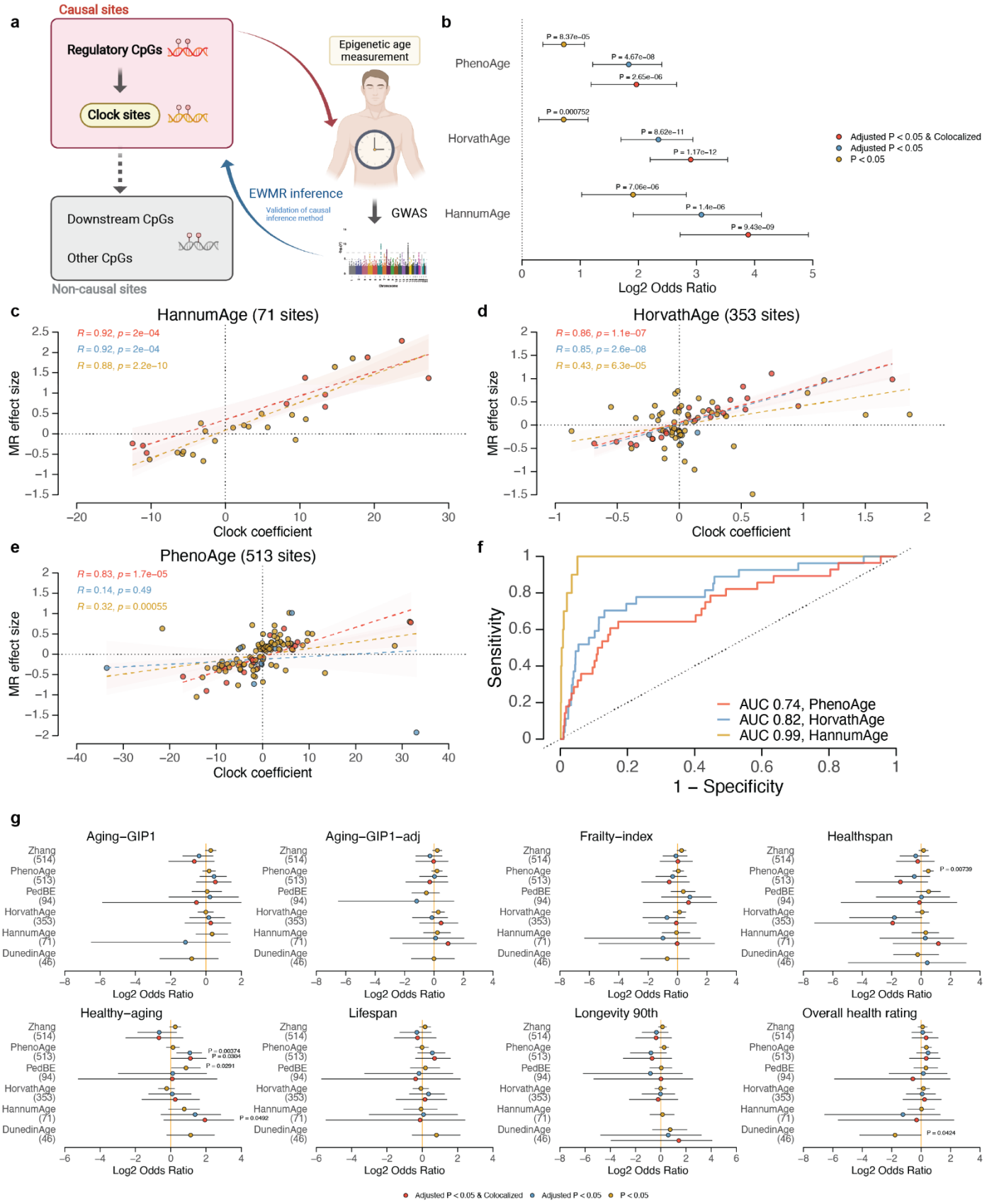
a
Causal sites
Regulatory CpGs
Clock sites
Downstream CpGs
Other CpGs
Non-causal sites
Epigenetic age measurement
EWMR inference
Validation of causal inference method
GWAS
b
PhenoAge
HorvathAge
HannumAge
P = 8.37e−05
P = 4.67e−08
P = 2.65e−06
P = 0.000752
P = 8.62e−11
P = 1.17e−12
P = 7.06e−06
P = 1.4e−06
P = 9.43e−09
Adjusted P < 0.05 & Colocalized
Adjusted P < 0.05
P < 0.05
Log2 Odds Ratio
c
HannumAge (71 sites)
R = 0.92, p = 2e−04
R = 0.92, p = 2e−04
R = 0.88, p = 2.2e−10
MR effect size
Clock coefficient
d
HorvathAge (353 sites)
R = 0.86, p = 1.1e−07
R = 0.85, p = 2.6e−08
R = 0.43, p = 6.3e−05
MR effect size
Clock coefficient
e
PhenoAge (513 sites)
R = 0.83, p = 1.7e−05
R = 0.14, p = 0.49
R = 0.32, p = 0.00055
MR effect size
Clock coefficient
f
Sensitivity
1 − Specificity
AUC 0.74, PhenoAge
AUC 0.82, HorvathAge
AUC 0.99, HannumAge
g
Aging−GIP1
Aging−GIP1−adj
Frailty−index
Healthspan
Healthy−aging
Lifespan
Longevity 90th
Overall health rating
Zhang (514)
PhenoAge (513)
PedBE (94)
HorvathAge (353)
HannumAge (71)
DunedinAge (46)
Log2 Odds Ratio
Adjusted P < 0.05 & Colocalized
Adjusted P < 0.05
P < 0.05

802 **Fig. 4**

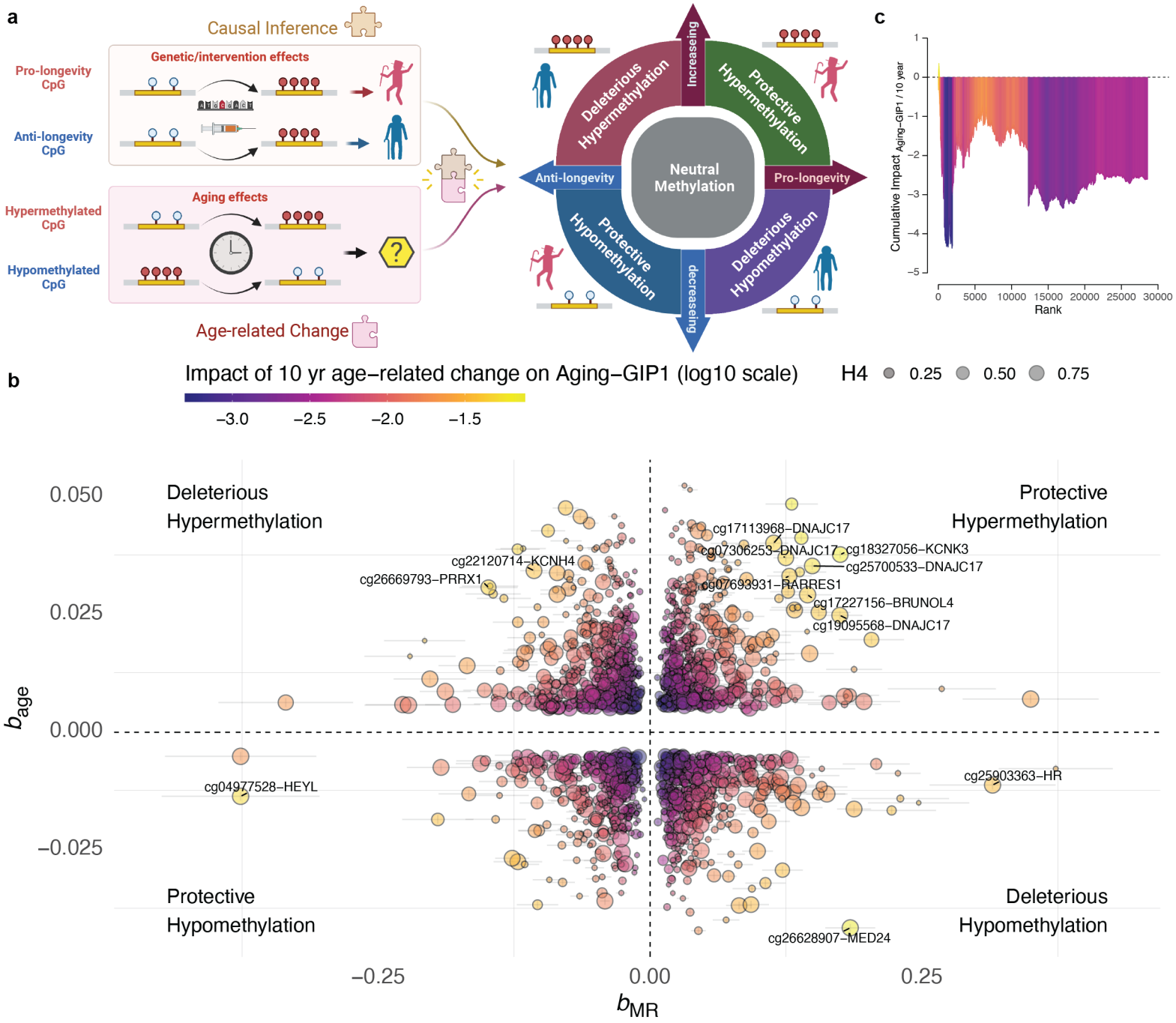
a
Causal Inference
Genetic/intervention effects
Pro-longevity CpG
Anti-longevity CpG
Aging effects
Hypermethylated CpG
Hypomethylated CpG
Age-related Change
Increaseing
Deleterious Hypermethylation
Protective Hypermethylation
Anti-longevity
Neutral Methylation
Pro-longevity
Protective Hypomethylation
Deleterious Hypomethylation
decreaseing
c
Cumulative Impact Aging−GIP1 / 10 year
Rank
b
Impact of 10 yr age−related change on Aging−GIP1 (log10 scale)
−3.0
−2.5
−2.0
−1.5
H4
0.25
0.50
0.75
Deleterious Hypermethylation
Protective Hypermethylation
Protective Hypomethylation
Deleterious Hypomethylation
cg17113968−DNAJC17
cg07306253−DNAJC17
cg18327056−KCNK3
cg25700533−DNAJC17
cg22120714−KCNH4
cg26669793−PRRX1
cg07693931−RARRES1
cg17227156−BRUNOL4
cg19095568−DNAJC17
cg04977528−HEYL
cg25903363−HR
cg26628907−MED24
b_{age}
b_{MR}

803 **Fig. 5**

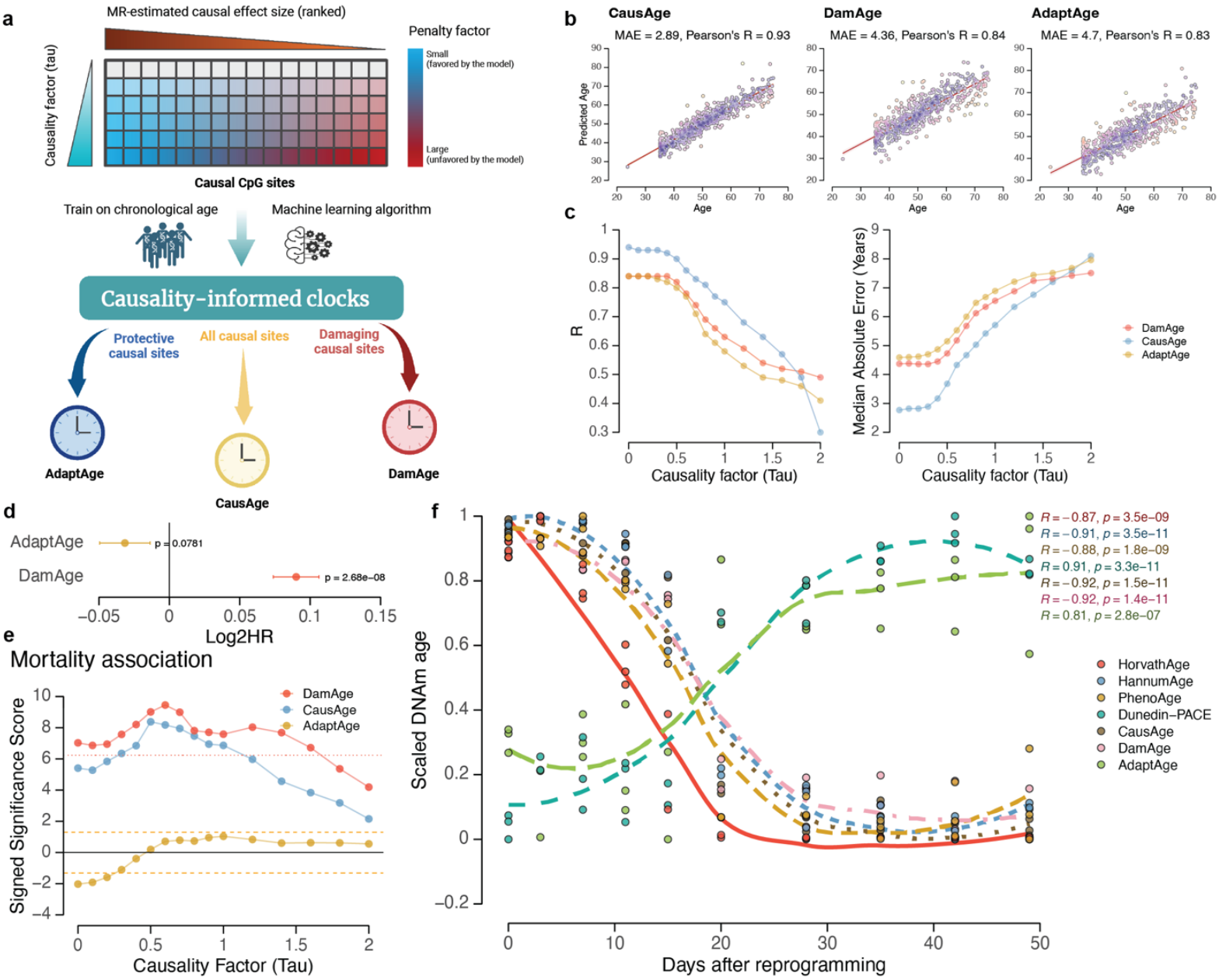
a
MR-estimated causal effect size (ranked)
Penalty factor
Small (favored by the model)
Large (unfavored by the model)
Causality factor (tau)
Causal CpG sites
Train on chronological age
Machine learning algorithm
Causality-informed clocks
Protective causal sites
All causal sites
Damaging causal sites
AdaptAge
CausAge
DamAge
b
CausAge
MAE = 2.89, Pearson's R = 0.93
DamAge
MAE = 4.36, Pearson's R = 0.84
AdaptAge
MAE = 4.7, Pearson's R = 0.83
Predicted Age
Age
c
R
Median Absolute Error (Years)
Causality factor (Tau)
DamAge
CausAge
AdaptAge
d
AdaptAge
p = 0.0781
DamAge
p = 2.68e−08
Log2HR
e
Mortality association
Signed Significance Score
Causality Factor (Tau)
DamAge
CausAge
AdaptAge
f
Scaled DNAm age
Days after reprogramming
R = −0.87, p = 3.5e−09
R = −0.91, p = 3.5e−11
R = −0.88, p = 1.8e−09
R = 0.91, p = 3.3e−11
R = −0.92, p = 1.5e−11
R = −0.92, p = 1.4e−11
R = 0.81, p = 2.8e−07
HorvathAge
HannumAge
PhenoAge
Dunedin−PACE
CausAge
DamAge
AdaptAge

804 **Fig. 6**

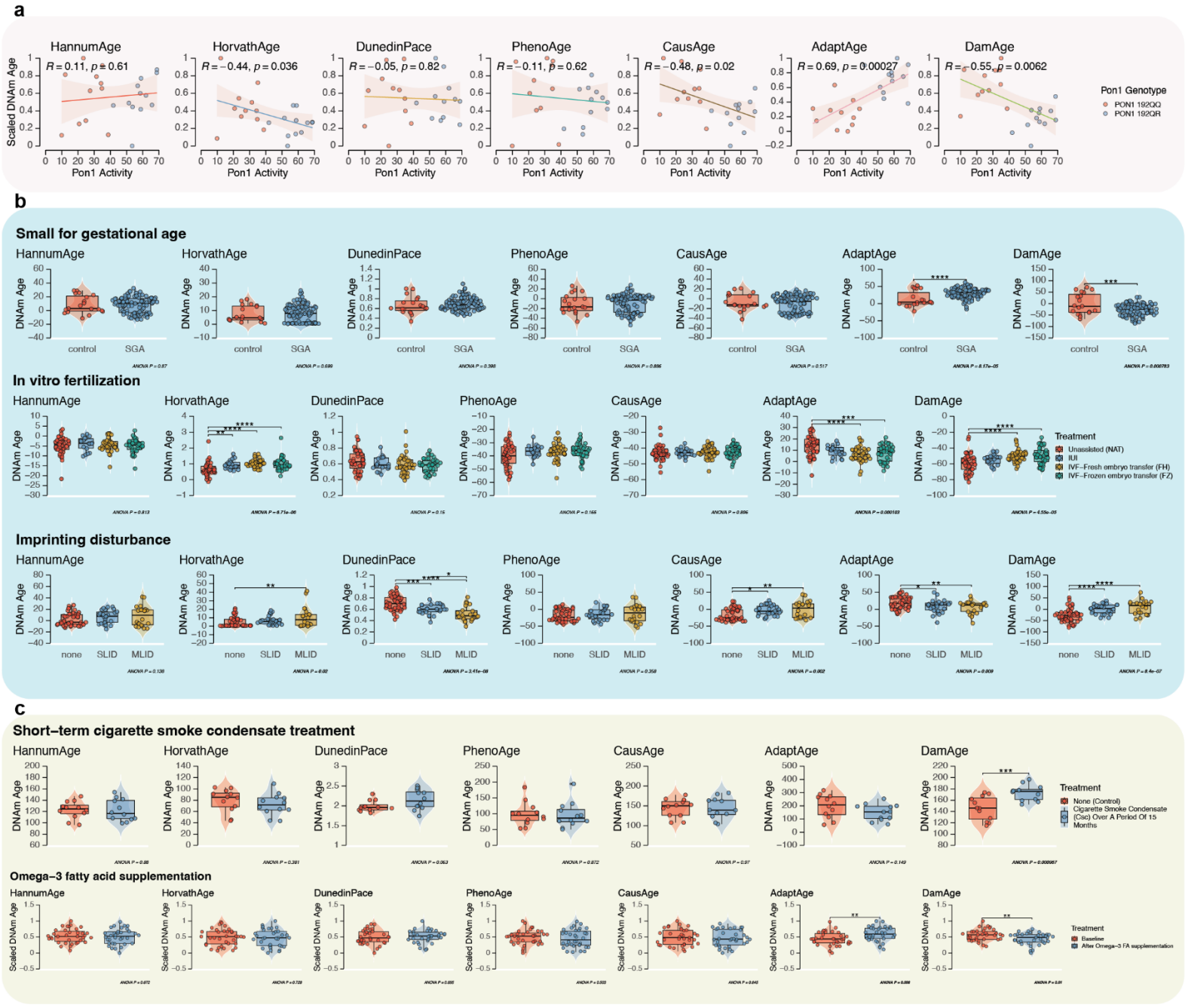
a
HannumAge
R = 0.11, p = 0.61
HorvathAge
R = −0.44, p = 0.036
DunedinPace
R = −0.05, p = 0.82
PhenoAge
R = −0.11, p = 0.62
CausAge
R = −0.48, p = 0.02
AdaptAge
R = 0.69, p = 0.00027
DamAge
R = −0.55, p = 0.0062
Scaled DNAm Age
Pon1 Activity
Pon1 Genotype
PON1 192QQ
PON1 192QR
b
Small for gestational age
DNAm Age
control
SGA
In vitro fertilization
Treatment
Unassisted (NAT)
IUI
IVF−Fresh embryo transfer (FH)
IVF−Frozen embryo transfer (FZ)
Imprinting disturbance
none
SLID
MLID
c
Short−term cigarette smoke condensate treatment
Treatment
None (Control)
Cigarette Smoke Condensate (Csc) Over A Period Of 15 Months
Omega−3 fatty acid supplementation
Scaled DNAm Age
Baseline
After Omega−3 FA supplementation